Article:

Research Article

Production and Digital Image Correlation Analysis of Titanium Foams with Different Pore Morphologies as a Bone-Substitute Material

Mohammed Shbeh ,[1] Elif Oner,[1] Ammar Al-Rubaye,[2] and Russell Goodall[1]

[1]*Department of Materials Science and Engineering, University of Sheffield, Sir Robert Hadfield Building, Mappin Street, Sheffield S1 3JD, UK*
[2]*Mechanical Engineering Department, University of Sheffield, Mappin Street, Sheffield S1 3JD, UK*

Correspondence should be addressed to Mohammed Shbeh; mohammed.shbeh@gmail.com

Ti foams are mesoporous structured materials that are characterized by their high surface area and interconnected porosity with a huge potential for biomedical applications. In this study, we investigated the production of titanium foams with different pore morphologies as a bone-substitute material via the addition of different amounts, shapes, and sizes of the space holder. Furthermore, we also carried out strain analysis using digital image correlation (DIC) in order to analyse the strain distribution across the porous samples. In addition, the nature of the relationship between the amount of the space holder added and final amount of porosity in the foams produced was also examined. The results demonstrated that the relationship between the space holder amount and porosity in the samples follows a complex one-phase exponential decay function in an increasing form. Our findings also suggest that the shape of the space holder does not play a significant role in dictating the porosity of the foams produced in the current study. However, the space holder's shape does have a substantial role in dictating the mechanical properties of the foams produced, where Ti foams produced using a cubic or irregular space holder were found to have a lower yield stresses than those made with the spherical space holder.

1. Introduction

Human bone is a complex composite material composed of organic and inorganic components. The organic part of the bone is comprised of a matrix polymer known as collagen, which is responsible for giving the bone its toughness, whereas the inorganic element of the bone has a similar chemical and crystal structure to that of a ceramic material, hydroxyapatite, and plays an important role in providing the bone with strength and stiffness [1, 2]. Bone tissue occurs in two forms or types in our bodies, and both of these forms have an anisotropic structure. The first type is the trabecular or spongy bone which is composed of an interconnected porous network of plates and rods arranged in various configurations, forming an open-celled foam [3, 4]. The second type is the cortical or compact bone characterized by

having a higher density, less porosity, and metabolic activity than that of a trabecular bone [5]. The two forms of bone can be normally found together in different arrangements and in such a manner so that the bone has a combination of excellent load-bearing ability derived from the spongy tissue and improved mechanical strength acquired from the cortical bone. For instance, the cortical bone constitutes the outer tubular shell of the long bones and the external surface of the small and flat bones, while the trabecular bone composes the internal surface of small bones, the ends of the long bones, and between the surfaces of flat bones [6]. In some cases, such as severe damage or osteoporotic fractures, bones need to be replaced. Successful replacement of such hard tissue with an anisotropic complex structure and mechanical properties can be challenging without the use of appropriate biocompatible and biomimetic materials.

Synthetic porous ceramic and polymer materials developed so far are usually unsuitable for replacing weight-bearing bones due to the inability to provide good energy absorption under load while having a porous structure that replicates that of the bone [7]. Hence, metals are more widely used for implants under such conditions. The three most popular materials currently used for biomedical implants are Ti-6Al-4V, Co-Cr-Mo, and 316 stainless steel. However, each of these alloys contains some elements which are reportedly cytotoxic. For example, Shettlemore and Bundy studied the toxicity of these three alloys and found that the most toxic was Co-Cr-Mo followed by 316 stainless steel, while Ti-6Al-4V is minimally toxic, which was attributed to the high toxicity of Cr, Ni, and Co elements in the former alloys [8]. Another study however reported that Ti-6Al-4V is synergistically toxic due to the occurrence of interaction between the titanium, aluminium, and vanadium [9]. Pure titanium is potentially a good candidate for biomedical hard tissue implants due to its excellent corrosion resistance, good biocompatibility, and low cytotoxicity. Nevertheless, the mismatch between the density and mechanical properties of the bone and dense Ti can be problematic and might lead to bone resorption and eventual failure [10]. One approach to address this challenge is through the development of porous Ti or Ti foams with a biomimetic structure. Titanium foams are advanced mesoporous structures characterized by their high surface area and interconnected porosity with a huge potential for biomedical applications including for bone [11], dental implants [12], and drug delivery systems [13]. The potential use of Ti foams as a bone-substitute material lies in the fact that their mechanical properties are tailorable depending on the amount of porosity in their structure and can be set to match that of the surrounding tissue or bone, thus avoiding the stress shielding problem [14]. Ti foams can be produced by several techniques, which have been recently reviewed [15]. However, metal injection moulding in combination with a space holder (MIM-SH) offers several advantages over other production techniques, including the ability to produce Ti foams with near net shape and intricate geometries, as well as the structure of the foams produced replicates that of the bone in having a denser outer layer and inner spongy layer [16]. Furthermore, the mesoporous structure of the foams produced can be tailored to be similar to that of the bone due to the possibility of controlling the characteristics of the space holder material used, which generates the pore structure. Thus, in this study, processing of Ti foams with different percentages of porosity as a bone-substitute material via the MIM-SH technique will be investigated, and the developed foams will be further tested under compression loading. Dynamic microstrain analysis will also be carried out using digital image correlation (DIC) in order to determine the distribution of strain across the porous samples.

2. Materials and Methods

2.1. Effect of Space Holder Amount on Porosity and Mechanical Properties.
In order to investigate the effect of the space holder percentage on the initial and final amount of porosity,

as well as mechanical strength of samples, five feedstocks with different volume percentages of the space holder, namely, 0, 17, 35, 52, and 60%, were prepared by mixing commercially pure Ti powder with a mean particle size of $74.9\,\mu$m and spherical in shape (Arcam AB, Sweden) with a multicomponent polymeric binder and spherical potassium chloride ($D_{50} = 366\,\mu$m) as a space holder. Although fine Ti powders with a particle size below $45\,\mu$m are typically used in injection moulding, coarse Ti powder can be advantageous, as it is less prone to contamination during processing, debinding, and sintering, and it can result in more intentionally induced micropores [17]. Nevertheless, the presence of such micropores can negatively affect the mechanical properties. It should be noted that we have previously assessed the use of the coarse Ti powder in MIM and its effect on the produced parts, including the interstitial elements [17, 18].

The percentage of solid loadings for all feedstocks prepared was similar and equal to 58% vol. The binder was composed of 70% polyethylene glycol 1500 (PEG), 25% PMMA, and 5% stearic acid. The composite feedstocks were mixed in a similar manner to our previous experiments and extruded twice using a vertical injection moulder before injecting cylindrical samples with a 10 mm in diameter and 13 mm in height at an injection temperature of 150°C and pressure of 45 MPa [18]. The initial porosity of each group of the green samples was determined by comparing the densities of five green samples measured by a helium pycnometer to that of the theoretical density, while the mechanical strength of the green samples was determined using a Zwick Z050 materials testing system at a strain rate of $0.001\,s^{-1}$. Compliance testing was carried out, and data were subtracted from the results. Several samples of each feedstock were then water debinded at 50°C and sintered at 1320°C for 2 h in order to investigate the effect of the space holder volume percentage on the final amount of porosity and mechanical strength of the samples under compression loading. The full details of the water debinding and sintering stages are reported elsewhere [18]. The final porosity and volume shrinkage in the sintered samples were determined by a helium pycnometer and Vernier caliper, after averaging five measurements for each group of samples.

2.2. Digital Image Correlation (DIC).
The DIC test for the porous samples was carried out in order to analyse the failure mechanism and try to visualise the extent of deformation that occurs in the samples during compression. Two groups of samples were tested. The first group of samples were those processed using feedstock with the 17% vol. space holder (low space holder percentage), while the second group of samples were those prepared using feedstocks with 52% vol. space holder (high space holder percentage). The samples were firstly painted with white paint from DecoArt, Stanford, USA, and then black speckled uniformly using a dual-action, siphon feed airbrush. Great difficulty was encountered during the white painting stage due to the porous nature of the samples and their high surface area, and the best results were achieved through the use of a high viscosity paint (20% solvent and 80% paint),

whereas less viscous paints either flowed off or were sucked into the pores of the sample. Samples with higher amount of porosity (those made with 60% space holder) were more challenging to paint as the paint did not have enough time to settle on the surface due to increased surface tension, whereas less porous samples get uniformly covered with the white paint, unlike high-porosity samples. Thus, two groups of samples with the best coating results were chosen for DIC analysis. Specially developed platens had to be used due to the small size of the samples and their poor visibility in the cameras when normal platens are used. The platens used were composed of two hardened steel screws with their heads ground and polished up to 2000 grit. The small platens were screwed into the universal testing machine, and samples were placed on them as demonstrated in Figure 1.

The software used for image analysis was LA Vision with a subset size of 17 and step size of 5. The subset size specifies the part of the image which is used to monitor the displacement between the taken images, while the step size restrains the spacing between points that are analysed during correlation [19].

2.3. Effect of the Shape of the Space Holder.

The influence of the space holder particle's shape and size on the initial and final amount of porosity in the feedstock and mechanical strength were investigated by preparing four different feedstocks with different particle shapes and sizes of the space holder, namely, cubic KCl particles with a mean particle size of 336 μm (CU336), cubic KCl with a mean particle size of 381 μm (CU381), spherical KCl with a mean particle size of 380 μm (SP380), and spherical KCl with a mean particle size of 607 μm (SP607). The potassium chloride was supplied by Sigma-Aldrich. The particle-size distributions for the KCl powders used were measured using a Malvern Mastersizer 3000 with the dry analysis method and are shown in Figure 2.

In order to compare the particle-size distribution width for the space holders used, the full width at the half maximum value was determined for each space holder by drawing a horizontal line at 50% of the maximum and finding the difference between the two values that intersects the drawn line (Figure 2(b)) [20]. It was found that SP380 and SP607 space holders had the highest full width at half maximum, as the values were 294.6 and 271.1 μm, respectively, compared to those for CU381 and CU336 space holders, which were 253.4 and 188.3 μm, respectively. Hence, spherical SP380 had the widest particle-size distribution compared to other space holders. The percentage of the solid content in the feedstocks prepared was 58%, of which 60% was KCl. The feedstocks were prepared and extruded using the same procedure mentioned previously. Several samples of each of those feedstocks before and after injection were taken and tested for porosity using a helium pycnometer at a pressure of approximately 0.07 MPa over 10 cycles. Several samples were then sintered from each feedstock at 1320°C for 2 h to check the percentage of final porosity in the foams produced. The average pore diameter for the samples sintered and their degree of roundness were determined using image analysis software (ImageJ, a public domain Java image processing program, https://www.imagej.nih.gov) by binarizing cross-sectional SEM images and measuring pore diameters using minimum and maximum Feret diameters and then averaging them. For Ti foams which have interconnected pores with no boundaries or cell walls among the pores, spherical particles with size equal to the average particle size of the Ti particles in the image were drawn in order to separate the two pores before estimating their pore size. This is demonstrated on an SEM image of a Ti foam with a porosity of approximately 64% in Figure 3(a) and can be taken as an example. The pores in the sample are interconnected with no cell walls in between, and thus particles were drawn in the image in order to separate the pores; the processed image after drawing of particles is illustrated in Figure 3(b). After that, each individual pore is selected through the use of the wand tracing tool of ImageJ, which traces the boundaries of objects with uniform colour (black in the case of pores) and added manually to the ROI manager after assigning them with designated numbers using the cell counter function in ImageJ in order to not count the same pore twice. Feret diameters are then measured and averaged for all of the pores using the measure function. The mechanical strength of the sintered samples under compression loading was assessed at a strain rate of $0.001 \, \text{s}^{-1}$. The yield strength for the samples was estimated using the 0.2% offset method.

3. Results and Discussion

3.1. Green Samples and Initial Porosity.

The presence of any initial porosity in the feedstock and in the samples before sintering (green samples) can hugely impact the green mechanical strength of the samples as well as their final mechanical properties. The amount of this porosity depends on several factors, such as the volume percentage of binder added to the mixture, particle size, and shape of the Ti powder as well as the temperature of extrusion and injection for both of the feedstock and samples, respectively. Good volume percentage of binder and low viscosity are required to achieve low initial porosity by efficiently wetting the Ti particles and bonding them together. However, increased amount of the binder can result in an increase in the volume shrinkage of samples. Therefore, a balance between those two must be reached for reduced initial porosity and accepted volume shrinkage.

Adding another material to the feedstock during mixing in addition to the Ti (such as the space holder) can make it more difficult for the binder to wet all of the particles without leaving voids, consequently resulting in an increased amount of initial porosity, depending on the mixing procedure. Thus, it is important to investigate the effect of adding the space holder to the samples on the initial porosity and green strength in order to assess the ability of these samples to withstand mechanical handling before debinding, as well as to make sure that this initial porosity is maintained at an acceptable level.

The results of the porosity analysis as well as the compression tests for the green samples are shown in Figure 4. It can be seen from Figure 4 that the initial porosity in the
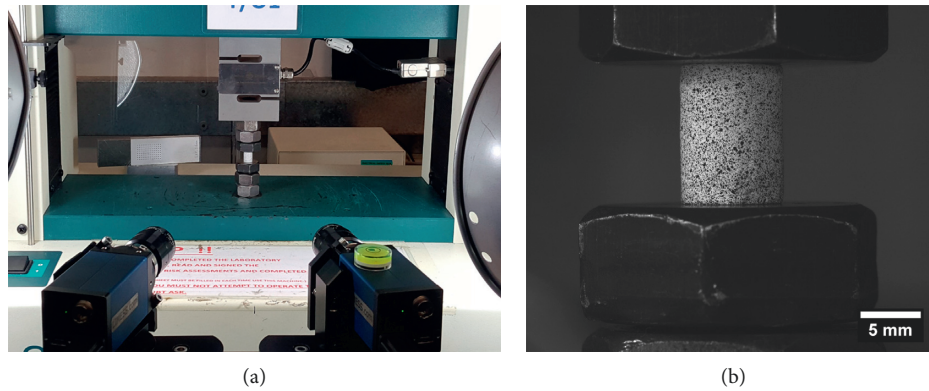
(a)

(b)

FIGURE 1: (a) DIC test setup; (b) porous sample in between two hardened steel screws.

(a)

(b)
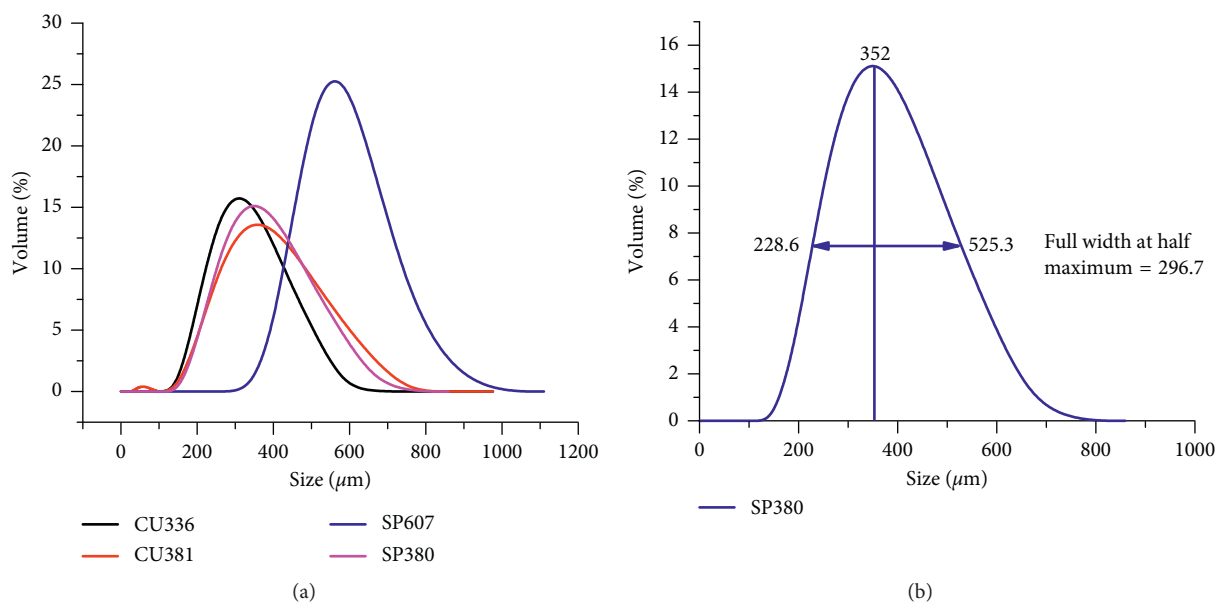
FIGURE 2: (a) The particle-size distribution of KCl is used, where CU336 is a cubic KCl with a mean particle size of 336 μm ($D_{10} = 217\,\mu$m, $D_{90} = 475\,\mu$m), CU381 is a cubic KCl with a mean particle size of 381 μm ($D_{10} = 224\,\mu$m, $D_{90} = 541\,\mu$m), SP607 is a spherical KCl with a mean particle size of 607 μm ($D_{10} = 468\,\mu$m, $D_{90} = 755\,\mu$m), and SP380 is a spherical KCl with a mean particle size of 380 μm ($D_{10} = 241\,\mu$m, $D_{90} = 544\,\mu$m). (b) An example for calculating the full width at half maximum for the space holder SP380.

samples generally increases slightly with the addition of the space holder, and there are no significant differences in the amount of initial porosity among samples with different volume percentages of space holder. The results of the mechanical tests showed that the green compressive strength of the samples decreases with the increasing amount of KCl powder in the samples, with the highest strength for samples having no space holder. The decrease in the strength with the increasing space holder percentage could be attributed to the large particle size of the KCl and its small surface area compared to the Ti powder resulting in weaker bonding to the polymeric binder. The strength of such composites made of polymer matrix with fillers like Ti and KCl is strongly dependent on the efficiency of the stress transfer between the polymer matrix and the mixture of Ti and KCl fillers, and this efficiency is reliant on how well these fillers are bonded to the polymer.

If the large KCl particles do not bond well to the polymer matrix, then inefficient load transfer occurs due to the inability of the large KCl particles to carry and transmit any load. Thus, the strength decreases with increasing KCl content. It is also generally reported that the strength of particle-reinforced polymer composites increases by reducing the particle size of the fillers and increasing their amount, up to a certain limit beyond which the strength decreases [21]. Hence, exchanging the smaller Ti particles with more weakly bonded, larger KCl particles would result in a deterioration in the strength of the composite. It should be noted that the fracture of the brittle KCl particles during compression loading can also adversely affect the green strength of composite green samples. However, there were no dramatic changes in terms of the shape of the stress-strain curves with and without KCl. It is worth noting that failure occurs in the samples by forming one or two cracks at 45°
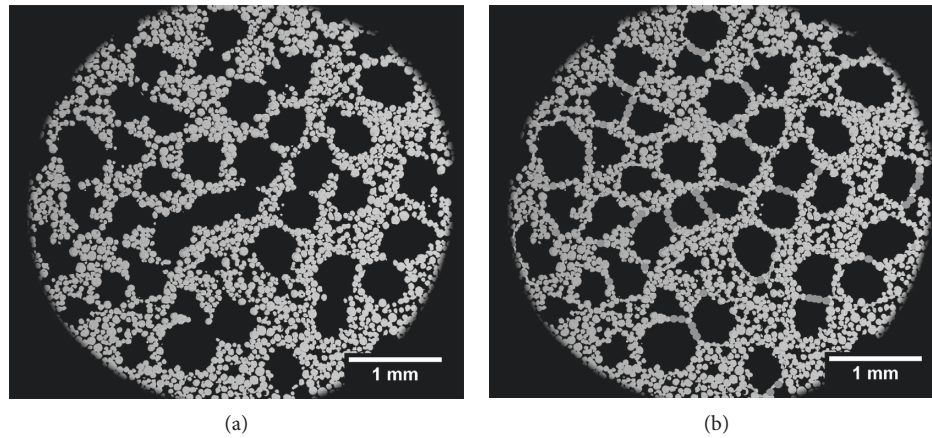
(a)

(b)

FIGURE 3: SEM image of a Ti foam: (a) before processing; (b) after defining the boundaries of the pores with spherical particles with size equal to the average particle size of the Ti particles.
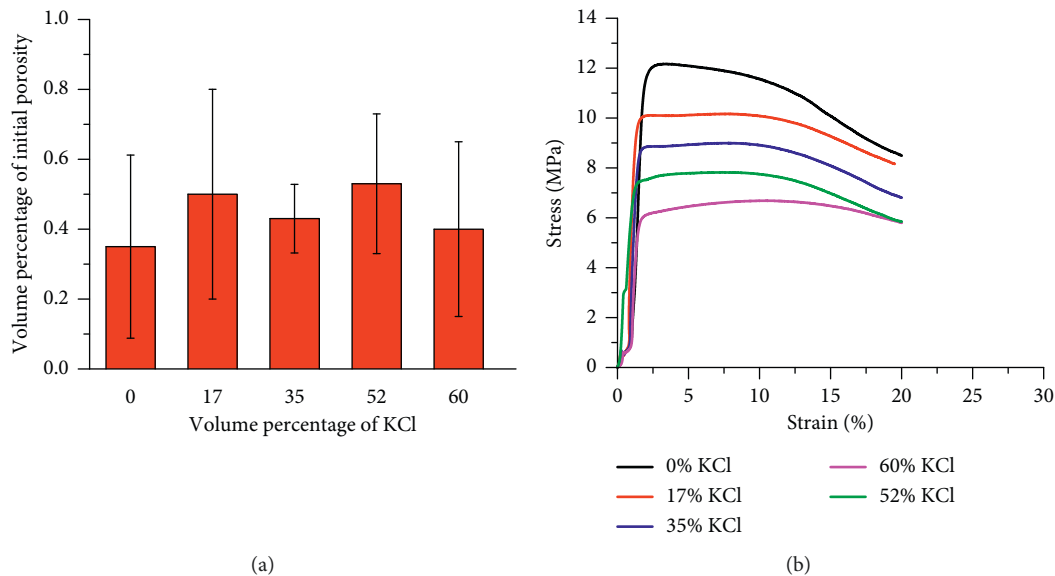

(a)

(b)

FIGURE 4: (a) The amount of initial porosity in the green samples with the space holder added; (b) the green strength of the samples with the space holder.

and these cracks grow gradually to the other end of the sample, as shown in Figure 5. In addition, it was also observed that KCl particles are ejected from the sample as the samples are compressed, and they settle on the platens of the compression testing machine, which can be taken as an evidence for the weak bonding between the KCl particles and the binder compared to the Ti particles, which stayed bonded to the binder. This is in a good agreement with our previous observation of the green samples after fracture, which is reported elsewhere [18].

3.2. Space Holder Percentage and the Amount of Final Porosity and Strength.

The volume percentage of final porosity in the samples depends strongly on the amount of the space holder added to the mixture as well as the sintering parameters. Sintering samples at high temperatures for longer times can

lead to better bonding between the Ti particles and the formation of complete necks, but at the same time, it can reduce pore volume, increase volume shrinkage, and result in closure of the pores. Thus, care must be taken during sintering of porous materials. The volume percentages of porosities for samples processed with the 0, 17, 35, 52, and 60% vol. space holder and their mechanical behaviour under compression loading are depicted in Figures 6(a) and 6(b).

It can be seen from Figure 6(a) that the relationship between the space holder amount added to the mixture and the final amount of porosity in the foams is not linear and follows a more complex one-phase exponential decay function in the increasing form, where the percentage of porosity in the samples seems to increase very rapidly at first and then the increase slows down to become asymptotic to an upper limit. This might be ascribed to increased volume shrinkage in the samples with increasing amount of the

Figure 5: Green samples with 17, 0, and 35 vol.% space holder (from left to right) after compression testing at a strain rate of 0.001 s^{-1}.

space holder. Increasing the space holder percentage will result in more connections between the KCl particles in the green samples and increased distance between the Ti particles surrounding the space holder. Thus, these Ti particles have to travel larger distances during sintering to initiate atomic bonds between each other and form cell walls, and these movements will consequently result in more volume shrinkage in the samples. This hypothesis could be supported by the amount of shrinkage measured in the sintered samples with the amount of space holder added, which is shown in Figure 6(c).

It was found that the amount of volume shrinkage in the samples increases exponentially with the increasing amount of space holder added. This could also be supported by the finding of Laptev et al. where they reported that with the increased amount of space holder added, the samples lose their stability and collapse under the action of gravity [22]. In addition, it was also noticed that the compressive strength of the foams was dramatically reduced with increasing amount of porosity (Figure 6(b)). Furthermore, the stress-strain curves for foams made with high volume percentage of porosity, particularly those made with 52 and 60% vol. space holder, showed clearly a very long plateau region before densification compared to those with low volume percentage of porosity, where the plateau region is shorter and not well defined, and the densification region is more prominent. Similar observations were reported in the literature for foams made by the space holder technique with porosities ranging from 45–68% by Esen and Bor [23], where they stated that the plateau region starts to disappear with reducing porosity in the samples, and the stress after yielding increases sharply. Foams with a large amount of porosity may have more uniform porous structure and undergo more uniform deformation to densification while those with a lower amount of porosity reach densification earlier.

In terms of the relationship between the relative density and the yield strength of the foams produced, the range of the data obtained seems to fit both linear and power-law regressions as shown in Figure 6(d) provided that the exponent for the latter regression is equal to 2.17 ± 0.25. It should be noted that the value is slightly higher than that predicted by Ashby for open-cell cellular materials, where

the value reported is 1.5, according to the following equation [24]:

$$\frac{\sigma_\text{f}}{\sigma_\text{s}} = C\left(\frac{\rho_\text{f}}{\rho_\text{s}}\right)^{3/2}, \tag{1}$$

where σ_f is the yield strength of the foam, σ_s is the yield strength of dense or solid Ti and was assumed to be 450 MPa for pure Ti [25], C is a proportionality constant (which is, however, well known to take slightly different values), and ρ_f and ρ_s are the densities of the foam and solid Ti, respectively. One study reported an exponent value of 3.57 and a proportionality constant of 2.13 for foams with porosities ranging from 45–96.8% produced by the space holder technique and ascribed the difference to parameters that are related to the mesostructure of the foams produced such as cell morphology, shape, and curvature of the cell walls [23]. The study also reported that the Gibson-Ashby model is only applicable for foams with volume percentage of porosity about 70% or higher. Although the value obtained here is closer than that reported in their study to the predicted value, the porosity is below 70% and this might have resulted in the small discrepancies in the exponent value. It is also worth noting that the data obtained here can also be fitted using linear regression and in agreement with the results reported by Wang et al. [26]. Hence, it is difficult to draw a firm conclusion and be certain of the overall trend of relative yield strength with relative density due to the limited range of porosity studied here, which might lead to a potential error in predicting the general trend.

Figure 7 shows that Ti foams processed by the current study have a much inferior yield strength compared to foams processed in the literature, and this can be attributed to the coarse Ti powder used here, as it results in a larger percentage of microporosity from the partial sintering of the Ti particles and the formation of microporous struts. This consequently reduces the ability of the samples to withstand high levels of stress, causing them to yield at lower stress values compared to samples processed in the literature by the same technique. The yield strength could be improved through the use of finer Ti powder. Yet, finer powders are more expensive and more prone to contamination, which in Ti can also result in changes to mechanical performance.

3.3. DIC Analysis Results. The results of the DIC analysis for compression of cylindrical samples of foams made with 17 and 52% KCl are shown in Figure 8. This shows sections of the curved surface analysed to produce strain maps (ε_1 shown), with the colour indicating the measured local strain. Thus, the red end of the spectrum indicates the regions where longitudinal strain is concentrated. It was found that much of the strain is concentrated at 45° in the samples in a similar manner to the failure of the green state, and thus failure is likely to occur by plastic deformation leading to the growth of cracks in these regions driven by the shear forces. Compared to foams made with 52% KCl, foams made with 17% KCl were much less deformed, which is expected due to reduced volume of porosity and improved mechanical strength.

Model	ExpDec1
Equation	$y = A1 * \exp(-x/t1)$
Plot	Porosity
$y0$	69.41848 ± 0.33
$A1$	-49.46206 ± 0.33
$t1$	26.99962 ± 0.33
Reduced chi-square	0.02921
R^2 (COD)	0.99994
Adj. R^2	0.99988

■ Data points
— Fitted curve

(a)

■ 60% KCl   — 17% KCl
— 52% KCl   — 0% KCl
— 35% KCl

(b)

Model	ExpDec1
Equation	$y = A1 * \exp(-x/t1)$
Plot	B
$y0$	14.59352 ± 3.096
$A1$	6.19835 ± 2.8594
$t1$	-50.01328 ± 3.096
Reduced chi-square	1.66918
R^2 CO	0.99584
Adj. R^2	0.99169

■ Data points
— Fitted curve

(c)

Equation	$y = a + b * x$
Intercept	-25 ± 3.096
Slope	0.85 ± 0.04
R-Square(COD)	0.99

Equation	$y = a * x \wedge b$
a	0.71 ± 0.07
b	2.17 ± 0.25
R^2 (COD)	0.97

■ Experimental data
— Linear fit of experimental data
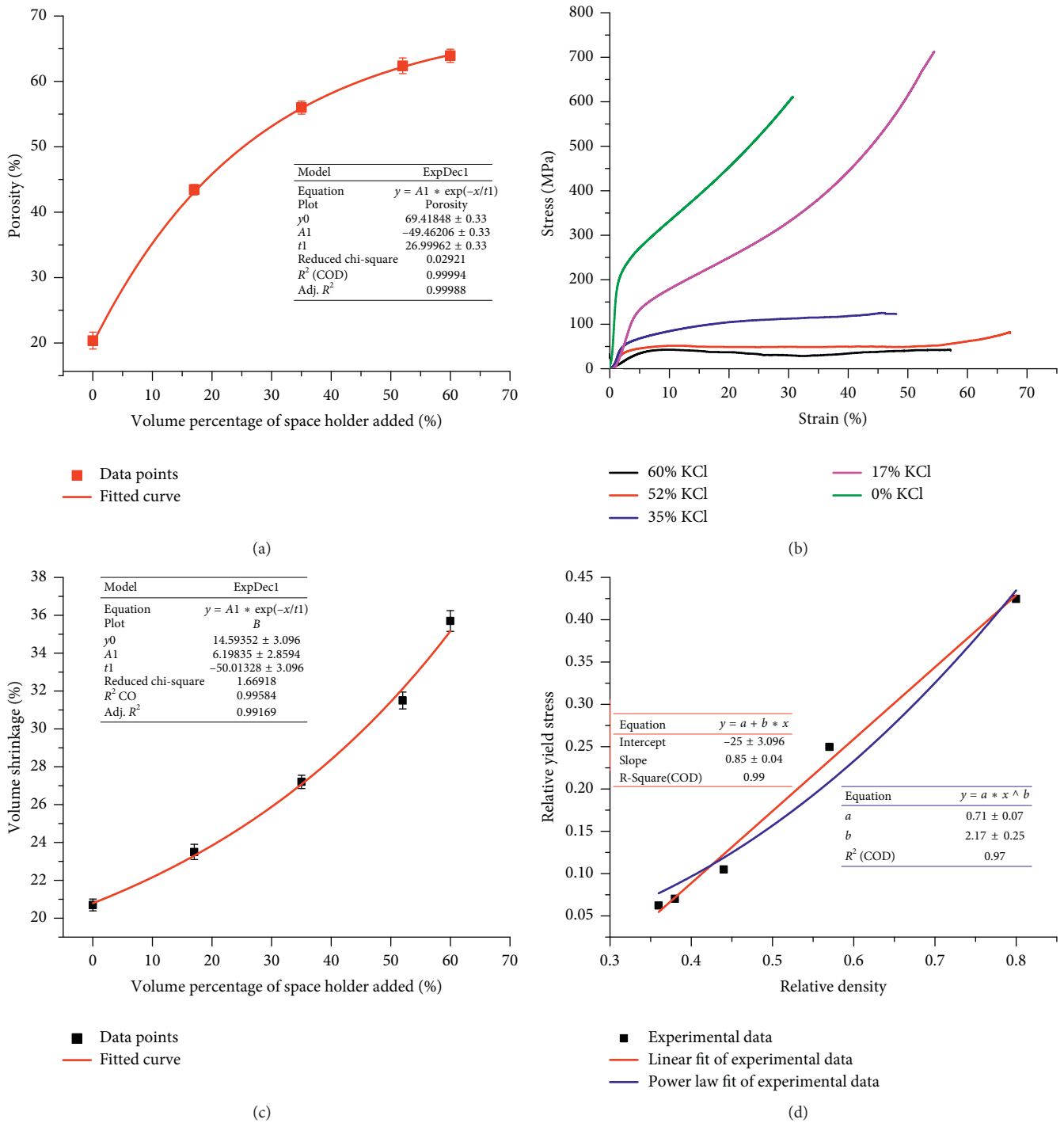— Power law fit of experimental data

(d)

FIGURE 6: (a) The relationship between the amount of space holder added and the final percentage of porosity in the sintered samples; (b) mechanical strength of samples with different amounts of porosity under compression; (c) the relationship between the amount of space holder added and the volume shrinkage of samples after sintering; (d) the change in the relative yield stress with the change in the relative density with two fitted curves, namely, linear and power law.

3.4. Effect of the Shape and Size of the Space Holder.

The percentage of initial porosity in the feedstock was found to be highest in the feedstock made with CU336, where it was equal to $1 \pm 0.2\%$, and this value reduced to $0.6 \pm 0.3\%$ after moulding of the samples. In comparison, other feedstocks had a negligible amount of porosity ranging between $0.4 \pm 0.2\%$ for feedstock made with CU381 to about 0.3 ± 0.2 and $0.1 \pm 0.1\%$ for feedstocks made with SP380 and SP607, respectively. Thus, it seems reasonable to say that the space holder particle size has some effect on the percentage of initial porosity, as well as the shape and size of the metal powder and the type of binder. The difference in the
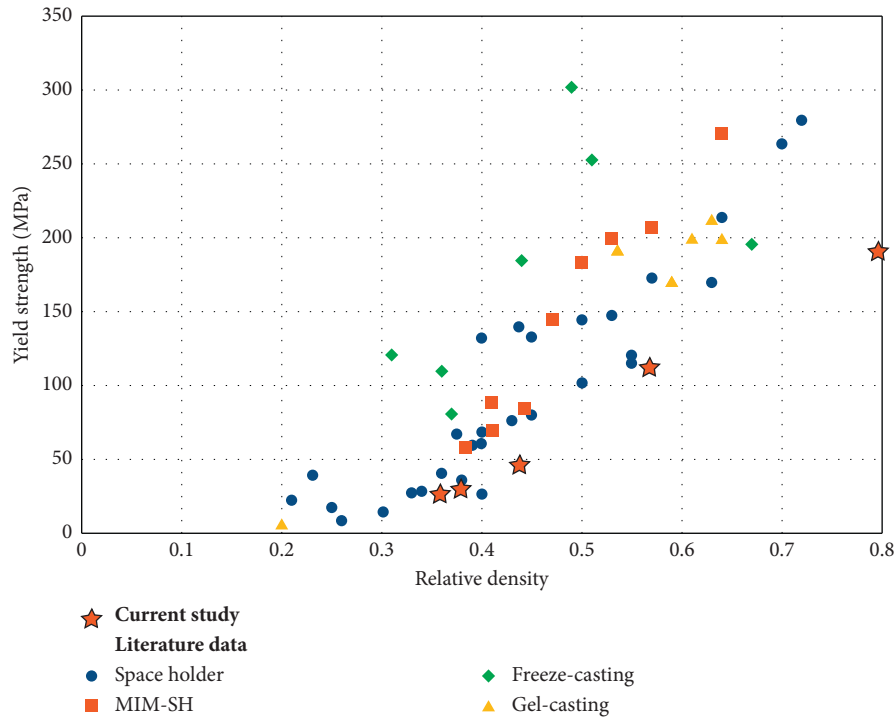
Figure 7: Comparison of yield strength between Ti foams processed by the current study and those reported in the literature for nonalloyed porous titanium with random structures. For ease of representation, data are grouped into the broad classes of methods, ignoring variations in how the technique is applied and pore size. Data are from [22, 27–49].
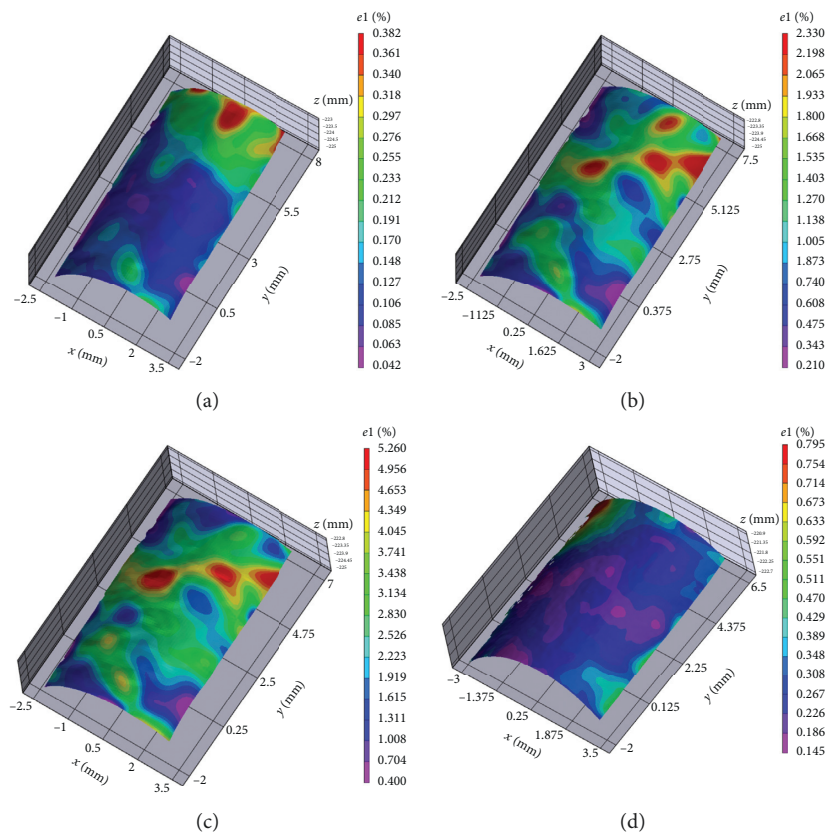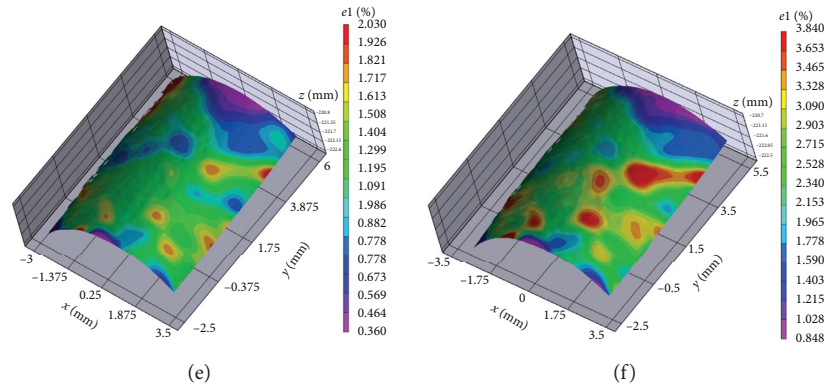

(a)

(b)

(c)

(d)

Figure 8: Continued.

(e)

(f)

FIGURE 8: The results of the DIC showing (a) Ti foam made by 52% KCl after 5% deformation, (b) Ti foam made by 52% KCl after 10% deformation, (c) Ti foam made by 52% KCl after 15% deformation, (d) Ti foam made by 17% KCl after 5% deformation, (e) Ti foam made by 17% KCl after 10% deformation, and (f) Ti foam made by 17% KCl after 15% deformation.

percentage of porosity can be attributed to the surface area of the particles. As the size of the KCl particle increases, the surface area to volume ratio decreases, thus keeping the volume percentage of porosity low by requiring less amount of binder to wet the KCl particles. Finer KCl particles, on the other hand, have higher surface area to volume ratio and require more binder to wet the particles. It is also worth noting that feedstocks made with the cubic space holder had generally higher green porosity than that for spherical, which might be owing to the Hopper-like shape of the cubic KCl, which makes it harder for the binder to wet the complete particles, resulting in a higher residual green porosity [18].

The results for porosity of samples after sintering are shown in Figure 9. It can be seen from Figure 9 that foams produced by the CU381 space holder had the highest porosity compared to other foams with a total average volume percentage of porosity of about 64.4% and a standard deviation of 0.4. This might be due to having a better packing density resulting in improved pore connections, by smaller KCl particles sitting among larger ones. Despite the fact that it had the widest particle-size distribution, samples processed with the space holder SP380 had slightly less porosity than those processed using the CU381 space holder and approximately equal to those made by CU336 and SP607. Thus, our findings seem to suggest that the shape of the space holder does not have a significant impact on the percentage of final porosity in our system, unlike what has been reported in the literature [49, 50].

SEM images of each group of the sintered samples which are made by different sizes and shapes of space holders are illustrated in Figure 10. All of the samples showed interconnected macropores with microporous cell walls surrounding them, and the shape of the pores approximately replicates the shape of the space holders used. The average pore diameter in the Ti foams produced and their degree of roundness were analysed and are summarised in Table 1. Generally, the average pore diameter for samples was noted to be somewhat lower than the average particle size of the space holder used. This could be

ascribed to pore shrinkage during sintering as the space holder is removed during water debinding leaving a network of open pores without any mechanical support during sintering. Similar findings have been reported in the literature for foams made by the space holder technique [51, 52]. In addition, the roundness and the uniformity of the shape of the pores in the foams produced with the spherical space holder were much higher than that for samples made with cubic space holder, and this could have wider implications for the mechanical properties of the foams produced.

The results of the compression testing of the Ti foams made by different shapes and sizes of space holders are shown in Figure 11. The results demonstrated that Ti foams made by the spherical space holder have higher yield stresses than those made with the cubic space holder. This might be due to the shape of pores present in the samples, where cracks can initiate more easily in the samples with irregular and angular pores compared to regular spherical pores, as they act as stress concentration sites with preformed crack tips or sharp corners, and thus samples yield at a lower stress value. Similar findings were reported in the literature for foams made with the space holder technique [53] and foams made by the entrapment and expansion of the argon gas technique [54]. It is important to point out that foams produced by the space holder with the narrowest particle-size distribution (CU336) had the lowest yield strength among the foams produced and is equal to 24 MPa, even though the foams produced had a lower porosity percentage than those processed with CU381. However, the yield strength for foams processed by CU381, SP380, and SP607 space holders were found to be 29, 32, and 34 MPa, respectively, and relatively higher, which seems to indicate that the width of the particle-size distribution of the space holder can play to some degree a role in dictating the yield strength.

SEM images of the foams after failure are shown in Figure 12. It was noted that all of the samples showed signs of a striated failure structure with some marks that resemble beach marks in fatigue failure. Furthermore, EDS results showed that samples were mainly composed of Ti with some
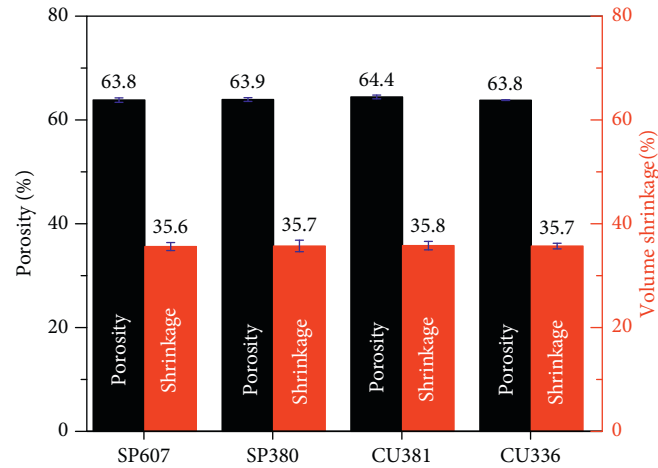
FIGURE 9: The relationship between the shape and size of space holder added and the final percentage of porosity and shrinkage in the sintered samples.
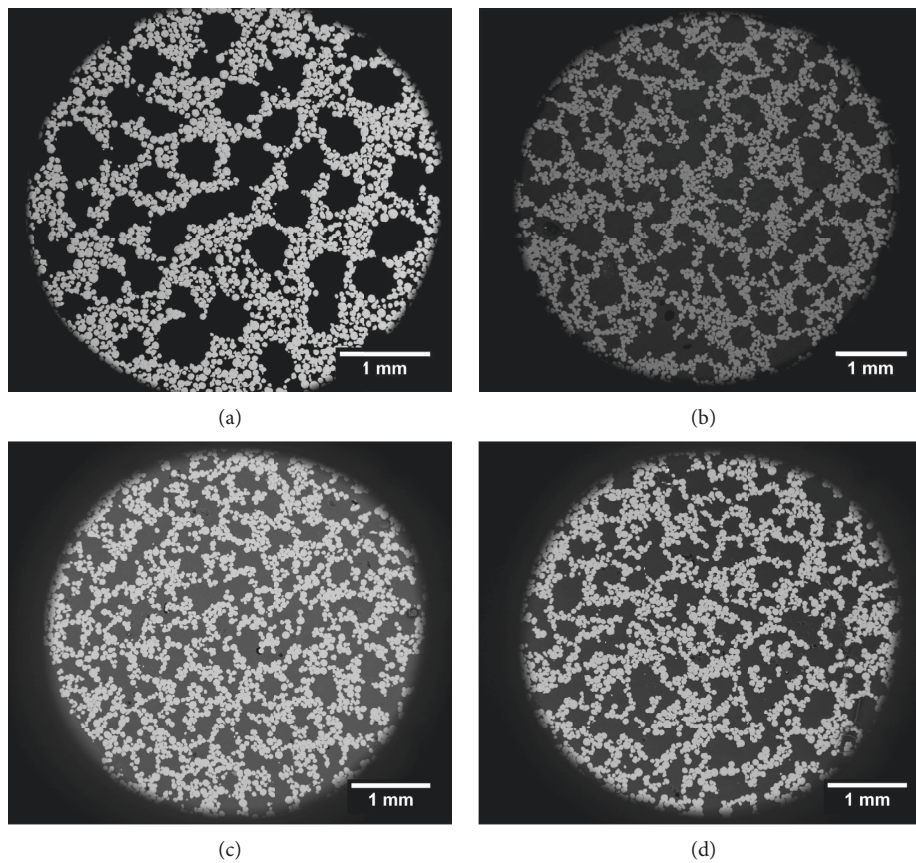

(a)

(b)

(c)

(d)

FIGURE 10: SEM images of (a) Ti foam made using SP607 space holder, (b) Ti foam made by SP380 space holder, (c) Ti foam made by CU336, and (d) Ti foam made by CU381.

TABLE 1: Average pore diameter in the Ti foams produced.

Feedstock used	Average pore diameter (μm)	Roundness
CU336	320	0.66
CU381	370	0.69
SP607	541	0.80
SP380	362	0.76

interstitial elements and no signs of other phases which are usually reported in foams due to the interaction of the space holder material with Ti [22, 50, 55]. This could be taken as an indication of the success of the process of removing the space holder by the ultrasonic water debinding technique, which has been previously reported by the authors [18].
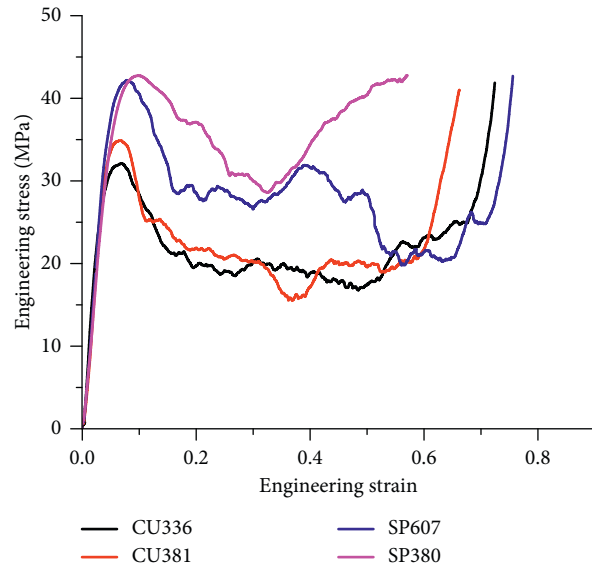
FIGURE 11: Mechanical strength of foams under compression testing at a strain rate of $0.001 \, \text{s}^{-1}$ made by cubic KCl with a mean particle size of $336 \, \mu$m (CU336), cubic KCl with a mean particle size of $381 \, \mu$m (CU381), spherical KCl with a mean particle size of $607 \, \mu$m (SP607), and spherical KCl with a mean particle size of $380 \, \mu$m (SP380).
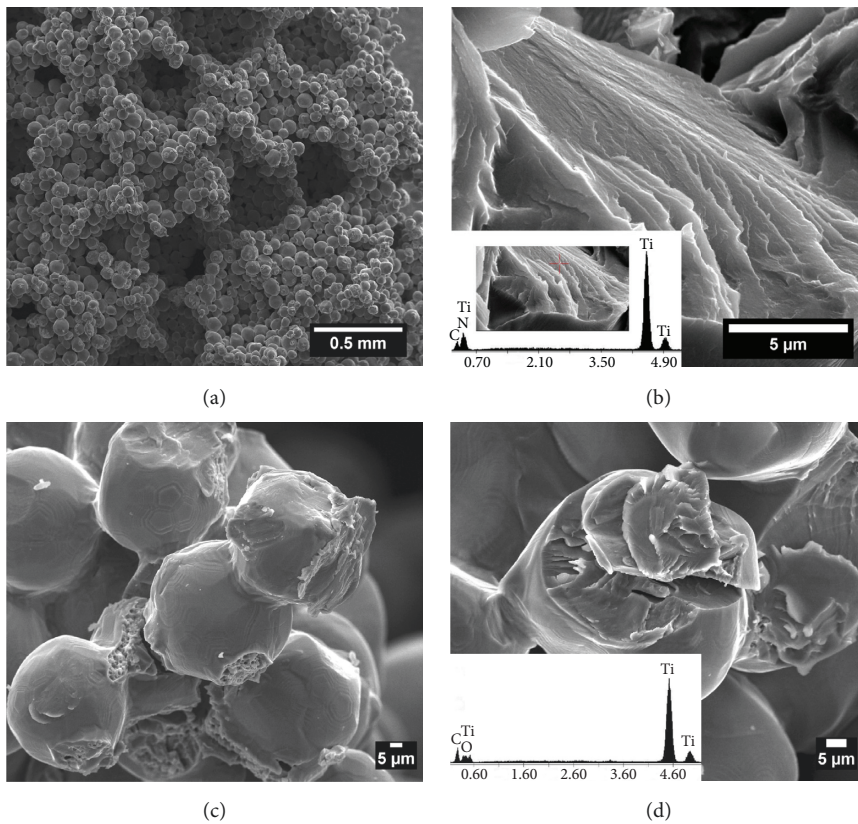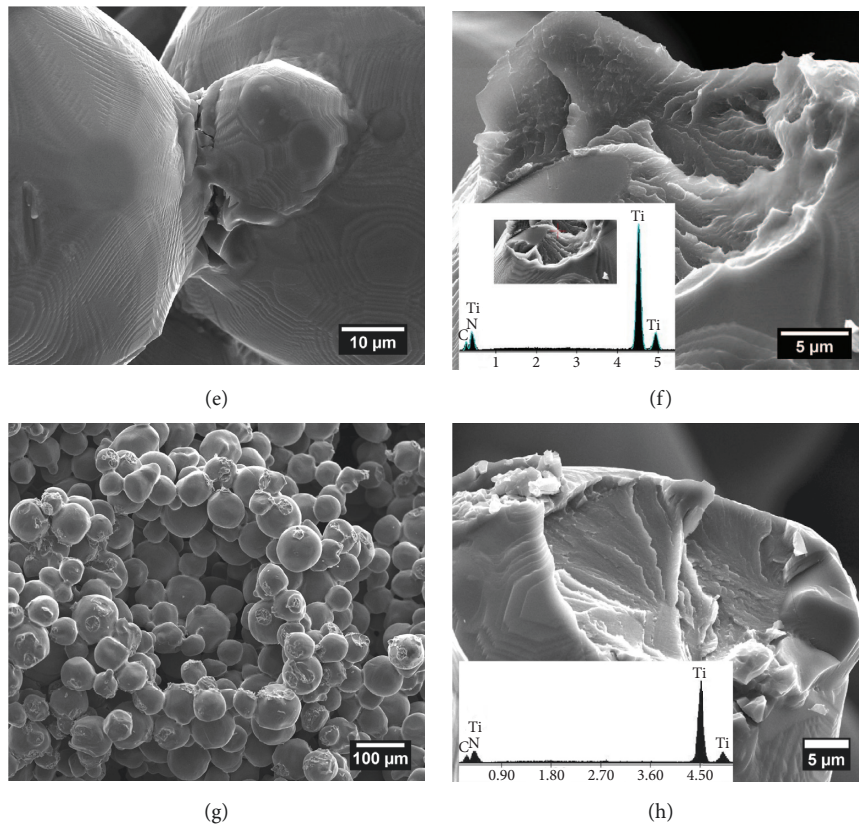

FIGURE 12: Continued.

(e)

(f)

(g)

(h)

Figure 12: SEM images of Ti foams after compression testing made with (a-b) SP607, (c-d) SP380, (e-f) CU336, and (g-h) CU381.

4. Conclusion

In this study, Ti foams with the potential for biomedical applications with different pore morphologies were produced by MIM-SH. Furthermore, the nature of the relationship between the amount of space holder added and the final amount of porosity in the foams produced was also examined. The results exhibited that the relationship follows a complex one-phase exponential decay function in the increasing form, where the percentage of porosity appears to dramatically increase by increasing the space holder amount at first, and then this increase slows down to become asymptotic to an upper limit. The latter trend is manifested by the occurrence of increased volume shrinkage by increasing the amount of space holder added, as this will result in more connections between the KCl particles and increased distances between the Ti particles. Thus, Ti particles have to travel larger distances during sintering to initiate atomic bonds and support the porous structure from collapse under the action of gravity. In addition, the effect of the space holder shape, size, and amount on the percentage of porosity and mechanical strength of the Ti foams produced was investigated. It was found that the shape of the space holder does not have a significant impact on the percentage of final porosity in our system. However, it does play an influential role in dictating the mechanical properties of the foams produced, where Ti foams produced by cubic space holder had lower yield stresses than those made with the spherical space holder. This can be ascribed to the shape of pores,

where irregular pores act as stress concentration sites with preformed crack tip. Thus, cracks initiate faster in the samples with irregular and angular pores compared to regular spherical pores, leading to yielding at lower levels of stress.

Data Availability

The data used to support the findings of this study are available from the corresponding author upon request.

Conflicts of Interest

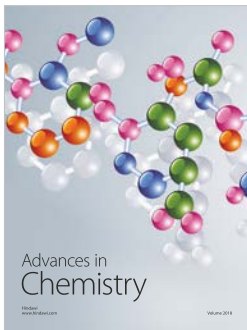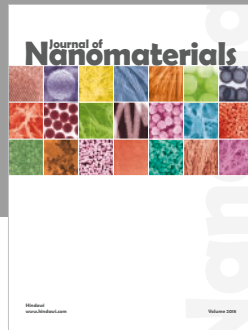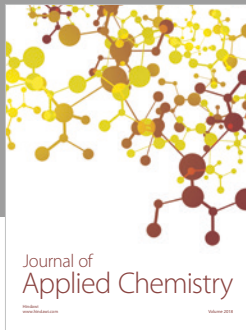The authors declare that they have no conflicts of interest.

Acknowledgments

References

[1] S. J. Mellon and K. E. Tanner, "Bone and its adaptation to mechanical loading: a review," *International Materials Reviews*, vol. 57, no. 5, pp. 235–255, 2013.

[2] P. A. Revell, "Quantitative methods in bone biopsy examination," in *Pathology of Bone*, pp. 87–111, Springer, Berlin, Germany, 1986.

[3] L. J. Gibson, "The mechanical behaviour of cancellous bone," *Journal of Biomechanics*, vol. 18, no. 5, pp. 317–328, 1985.

[4] I. Singh, "The architecture of cancellous bone," *Journal of Anatomy*, vol. 127, no. 2, pp. 305–310, 1978.

[5] B. Clarke, "Normal bone anatomy and physiology," *Clinical Journal of the American Society of Nephrology*, vol. 3, no. 3, pp. S131–S139, 2008.

[6] M. Yaszemski, R. G. Payne, W. C. Hayes, R. Langer, and A. G. Mikos, "Evolution of bone transplantation: molecular, cellular and tissue strategies to engineer human bone," *Biomaterials*, vol. 17, no. 2, pp. 175–185, 1996.

[7] H. Petite, V. Viateau, W. Bensaïd et al., "Tissue-engineered bone regeneration," *Nature Biotechnology*, vol. 18, no. 9, pp. 959–963, 2000.

[8] M. G. Shettlemore and K. J. Bundy, "Toxicity measurement of orthopedic implant alloy degradation products using a bioluminescent bacterial assay," *Journal of Biomedical Materials Research*, vol. 45, no. 4, pp. 395–403, 1999.

[9] L. Lucas, J. Lemons, and R. Buchanan, "Biocompatibility evaluations of Fe, Co and Ti base alloys," in *Proceedings of Transactions of the Annual Meeting of the Society for Biomaterials in Conjunction with the Interna*, Birmingham, AL, USA, April–May 1983.

[10] J. Xiong, Y. Li, X. Wang, P. Hodgson, and C. Wen, "Mechanical properties and bioactive surface modification via alkali-heat treatment of a porous Ti-18Nb-4Sn alloy for biomedical applications," *Acta Biomaterialia*, vol. 4, no. 6, pp. 1963–1968, 2008.

[11] A. Bansiddhi, T. D. Sargeant, S. I. Stupp, and D. C. Dunand, "Porous NiTi for bone implants: a review," *Acta Biomaterialia*, vol. 4, no. 4, pp. 773–782, 2008.

[12] K. Asaoka, N. Kuwayama, O. Okuno, and I. Miura, "Mechanical properties and biomechanical compatibility of porous titanium for dental implants," *Journal of Biomedical Materials Research*, vol. 19, no. 6, pp. 699–713, 1985.

[13] H. Lee, J. Hyun-Do, K. Min-Ho, S. Ju-Ha, and K. Hyoun-Ee, "Ti-based functionally graded porous structure for dual drug delivery system," *Frontiers in Bioengineering and Biotechnology*, vol. 4, 2016.

[14] M. M. Shbeh and R. Goodall, "Open pore titanium foams via metal injection molding of metal powder with a space holder," *Metal Powder Report*, vol. 71, no. 6, pp. 450–455, 2016.

[15] M. M. Shbeh and R. Goodall, "Open celled porous titanium," *Advanced Engineering Materials*, vol. 19, no. 11, article 1600664, 2017.

[16] M. M. Shbeh and R. Goodall, "Single- and multi-layered porous titanium via metal injection moulding," *Advanced Materials Letters*, vol. 8, no. 4, pp. 500–505, 2017.

[17] M. Menhal Shbeh, A. Yerokhin, and R. Goodall, "Microporous titanium through metal injection moulding of coarse powder and surface modification by plasma oxidation," *Applied Sciences*, vol. 7, no. 1, p. 105, 2017.

[18] M. M. Shbeh and R. Goodall, "Design of water debinding and dissolution stages of metal injection moulded porous Ti foam production," *Materials and Design*, vol. 87, pp. 295–302, 2015.

[19] Correlated Solutions, *VIC-3D 2010: Testing Guide*, Correlated Solutions, Irmo, SC, USA, 2010.

[20] B. B. Weiner, *What is a Continuous Particle Size Distribution*, Brookhaven Instruments Corporation White Paper, Holtsville, NY, USA, 2011.

[21] S. Y. Fu, X. Q. Feng, B. Lauke, and Y. W. Mai, "Effects of particle size, particle/matrix interface adhesion and particle loading on mechanical properties of particulate-polymer composites," *Composites Part B: Engineering*, vol. 39, no. 6, pp. 933–961, 2008.

[22] A. M. Laptev, N. F. Daudt, O. Guillon, and M. Bram, "Increased shape stability and porosity of highly porous injection-molded titanium parts," *Advanced Engineering Materials*, vol. 17, no. 11, pp. 1579–1587, 2015.

[23] Z. Esen and Ş. Bor, "Processing of titanium foams using magnesium spacer particles," *Scripta Materialia*, vol. 56, no. 5, pp. 341–344, 2007.

[24] M. F. Ashby and R. F. M. Medalist, "The mechanical properties of cellular solids," *Metallurgical Transactions A*, vol. 14, no. 9, pp. 1755–1769, 1983.

[25] V. Venkatesh and R. R. Boyer, *Proceedings of the 13th World Conference on Titanium*, John Wiley & Sons, Hoboken, NJ, USA, 2016.

[26] X. H. Wang, J. S. Li, R. Hu, H. C. Kou, and L. Zhou, "Mechanical properties of porous titanium with different distributions of pore size," *Transactions of Nonferrous Metals Society of China*, vol. 23, no. 8, pp. 2317–2322, 2013.

[27] M. Bram et al., "Application of powder metallurgy for the production of highly porous functional parts with open porosity," *Materials Science Forum*, vol. 29, pp. 119–122, 2005.

[28] S. C. P. Cachinho and R. N. Correia, "Titanium porous scaffolds from precursor powders: rheological optimization of TiH2 slurries," *Powder Technology*, vol. 178, no. 2, pp. 109–113, 2007.

[29] L. J. Chen, T. Li, Y. M. Li, H. He, and Y. H. Hu, "Porous titanium implants fabricated by metal injection molding," *Transactions of Nonferrous Metals Society of China*, vol. 19, no. 5, pp. 1174–1179, 2009.

[30] B. Dabrowski, W. Swieszkowski, D. Godlinski, and K. J. Kurzydlowski, "Highly porous titanium scaffolds for orthopaedic applications," *Journal of Biomedical Materials Research Part B: Applied Biomaterials*, vol. 95B, no. 1, pp. 53–61, 2010.

[31] K. A. Erk, D. C. Dunand, and K. R. Shull, "Titanium with controllable pore fractions by thermoreversible gelcasting of TiH2," *Acta Materialia*, vol. 56, no. 18, pp. 5147–5157, 2008.

[32] T. Imwinkelried, "Mechanical properties of open-pore titanium foam," *Journal of Biomedical Materials Research Part A*, vol. 81A, no. 4, pp. 964–970, 2007.

[33] P. Jenei, H. Choi, A. Tóth, H. Choe, and J. Gubicza, "Mechanical behavior and microstructure of compressed Ti foams synthesized via freeze casting," *Journal of the Mechanical Behavior of Biomedical Materials*, vol. 63, pp. 407–416, 2016.

[34] M. Khodaei, M. Meratian, and O. Savabi, "Effect of spacer type and cold compaction pressure on structural and mechanical properties of porous titanium scaffold," *Powder Metallurgy*, vol. 58, no. 2, pp. 152–160, 2015.

[35] Y. Li, Z. M. Guo, J. J. Hao, and S. B. Ren, "Gelcasting of porous titanium implants," *Powder Metallurgy*, vol. 51, no. 3, pp. 231–236, 2013.

[36] A. Mansourighasri, N. Muhamad, and A. B. Sulong, "Processing titanium foams using tapioca starch as a space holder," *Journal of Materials Processing Technology*, vol. 212, no. 1, pp. 83–89, 2012.

[37] D. P. Mondal, M. Patel, H. Jain, A. K. Jha, S. Das, and R. Dasgupta, "The effect of the particle shape and strain rate on microstructure and compressive deformation response of pure Ti-foam made using acrowax as space holder," *Materials Science and Engineering: A*, vol. 625, pp. 331–342, 2015.

[38] S. Muñoz, J. Pavón, J. A. Rodríguez-Ortiz, A. Civantos, J. P. Allain, and Y. Torres, "On the influence of space holder in the development of porous titanium implants: mechanical, computational and biological evaluation," *Materials Characterization*, vol. 108, pp. 68–78, 2015.

[39] W. Niu, C. Bai, G. Qiu, and Q. Wang, "Processing and properties of porous titanium using space holder technique," *Materials Science and Engineering: A*, vol. 506, no. 1-2, pp. 148–151, 2009.

[40] J. Rivard, V. Brailovski, S. Dubinskiy, and S. Prokoshkin, "Fabrication, morphology and mechanical properties of Ti and metastable Ti-based alloy foams for biomedical applications," *Materials Science and Engineering: C*, vol. 45, pp. 421–433, 2014.

[41] R. Singh, P. D. Lee, J. R. Jones et al., "Hierarchically structured titanium foams for tissue scaffold applications," *Acta Biomaterialia*, vol. 6, no. 12, pp. 4596–4604, 2010.

[42] N. Tuncer, M. Bram, A. Laptev, T. Beck, A. Moser, and H. P. Buchkremer, "Study of metal injection molding of highly porous titanium by physical modeling and direct experiments," *Journal of Materials Processing Technology*, vol. 214, no. 7, pp. 1352–1360, 2014.

[43] C. Wang, H. Chen, X. Zhu, Z. Xiao, K. Zhang, and X. Zhang, "An improved polymeric sponge replication method for biomedical porous titanium scaffolds," *Materials Science and Engineering: C*, vol. 70, pp. 1192–1199, 2017.

[44] X. H. Wang, J. S. Li, R. Hu, and H. C. Kou, "Mechanical properties and pore structure deformation behaviour of biomedical porous titanium," *Transactions of Nonferrous Metals Society of China*, vol. 25, no. 5, pp. 1543–1550, 2015.

[45] C. Xiang, Y. Zhang, Z. Li, H. Zhang, Y. Huang, and H. Tang, "Preparation and compressive behavior of porous titanium prepared by space holder sintering process," *Procedia Engineering*, vol. 27, pp. 768–774, 2011.

[46] B. Ye and D. C. Dunand, "Titanium foams produced by solid-state replication of NaCl powders," *Materials Science and Engineering: A*, vol. 528, no. 2, pp. 691–697, 2010.

[47] S. W. Yook, H. D. Jung, C. H. Park et al., "Reverse freeze casting: a new method for fabricating highly porous titanium scaffolds with aligned large pores," *Acta Biomaterialia*, vol. 8, no. 6, pp. 2401–2410, 2012.

[48] S. W. Yook, B. H. Yoon, H. E. Kim, Y. H. Koh, and Y. S. Kim, "Porous titanium (Ti) scaffolds by freezing TiH2/camphene slurries," *Materials Letters*, vol. 62, no. 30, pp. 4506–4508, 2008.

[49] E. Carreño-Morelli, M. Rodríguez-Arbaizar, A. Amherd, and J. E. Bidaux, "Porous titanium processed by powder injection moulding of titanium hydride and space holders," *Powder Metallurgy*, vol. 57, no. 2, pp. 93–96, 2014.

[50] A. Ghasemi, S. R. Hosseini, and S. K. Sadrnezhaad, "Pore control in SMA NiTi scaffolds via space holder usage," *Materials Science and Engineering: C*, vol. 32, no. 5, pp. 1266–1270, 2012.

[51] M. Bram, C. Stiller, H. P. Buchkremer, D. Stöver, and H. Baur, "High-porosity titanium, stainless steel, and superalloy parts," *Advanced Engineering Materials*, vol. 2, no. 4, pp. 196–199, 2000.

[52] T. F. Hong, Z. X. Guo, and R. Yang, "Fabrication of porous titanium scaffold materials by a fugitive filler method," *Journal of Materials Science: Materials in Medicine*, vol. 19, no. 12, pp. 3489–3495, 2008.

[53] D. S. Li, Y. P. Zhang, G. Eggeler, and X. P. Zhang, "High porosity and high-strength porous NiTi shape memory alloys with controllable pore characteristics," *Journal of Alloys and Compounds*, vol. 474, no. 1-2, pp. L1–L5, 2009.

[54] H. Li, S. M. Oppenheimer, S. I. Stupp, D. C. Dunand, and L. C. Brinson, "Effects of pore morphology and bone ingrowth on mechanical properties of microporous titanium as an orthopaedic implant material," *Materials Transactions*, vol. 45, no. 4, pp. 1124–1131, 2004.

[55] T. Aydogmus and S. Bor, "Processing of porous TiNi alloys using magnesium as space holder," *Journal of Alloys and Compounds*, vol. 478, no. 1-2, pp. 705–710, 2009.